2016 NDIA GROUND VEHICLE SYSTEMS ENGINEERING AND TECHNOLOGY SYMPOSIUM
MODELING & SIMULATION, TESTING AND VALIDATION (MSTV) TECHNICAL SESSION
AUGUST 2-4, 2016 - NOVI, MICHIGAN

MODELING FRAGMENTATION OF A 155MM ARTILLERY SHELL IED IN A BURIED MINE BLAST EVENT

James G. Rasico
Navistar Defense
Madison Heights, MI

Craig A. Newman
Navistar Defense
Madison Heights, MI

Morten Rikard Jensen
CertaSIM, LLC
Castro Valley, CA

ABSTRACT

The shapes of Improvised Explosive Devices (IED) used by insurgents in recent conflicts are complex and can take many forms. To model unique shapes that are embedded in the soil, in addition to the actual shape of the High Explosive (HE), adds to the complexity of simulating the mine blast event. By considering an artillery shell as the container, further complicates the analysis because fragmentation of the shell has to be included. Unfortunately, this complex IED is not uncommon and in order to develop protective structures for our soldiers and civilians, finite element techniques are employed. The work presented is an investigation of how to do this modeling using the explicit non-linear transient finite element software, the IMPETUS Afea Solver®. The first step is a large sensitivity study of an explosive driven expansion of a simple cylinder and the outcome influence of nine design variables, leading to hundreds of computational hours. The modeling approach chosen for the HE is the discrete particle method (DPM). Applying the knowledge obtained from the expanding cylinder simulations, a model was created to simulate the explosion of a buried mine in the form of a structurally representative IED. The structure for the IED resembles a M795 artillery shell. To capture the fragmentation, the node splitting algorithm available in the IMEPTUS solver is used. The soil and HE are represented as discrete particles and modeled using the IMPETUS DPM algorithm. The blast ejecta target structure utilized is a modified model of the TARDEC Generic Vehicle Hull containing a seated IMPETUS Afea Hybrid III 50th Percentile Dummy.

INTRODUCTION

Improvised Explosive Devices (IED's) used by insurgents have become an effective device to inflict harm and cause destabilization. The cost of dealing with the IED threat is both immediate and enduring in human and financial terms. Military and civilian casualties may result in loss of life, limb, or diminished physical or mental capacity. There is also a tremendous financial cost burden for individuals and governments tasked with the long-term care of IED event survivors. Militaries spend ever greater portions of their limited budgets for hospitalization and disability care, as well as funding the development of safer environments, fixed and mobile, for soldiers and personnel in locations with active insurgencies.

The detonation of an IED produces explosive pressure, ejecta, and fragmentation, all of which may be harmful and damaging to its target. An IED may be placed in different media (air, soil, etc.) and take the form of many diverse shapes depending on what is used as the container for the high explosive (HE). In [1], a pile of cleared IED's are displayed, demonstrating a myriad of containers that have been used, including oil cans, jugs, coolers, and artillery shells. The artillery shell is especially dangerous because it is designed to parse into a barrage of metal shell fragments, many of which have combined mass and velocity sufficient to penetrate protective armor. Simulation methods using finite element techniques are frequently used to evaluate explosive pressure and/or ejecta effects on vehicle armor during design process, but have not included the addition of

artillery shell fragmentation as software algorithms lacked the robustness necessary to replicate the event physics.

This paper presents a modeling strategy for simulating a buried mine blast event where the IED is a 155mm M795 artillery shell and HE, soil "ejecta," and fragmentation are present. The HE and soil are modeled using the discrete particle method (DPM) that is implemented in the IMPETUS Afea Solver®, an explicit non-linear transient dynamic finite element solver. The shell casing and vehicle hull are modeled using solid elements and will take advantage of the "node splitting" algorithm to accurately account for damage, crack propagation, and fragmentation of the artillery shell. Buried mine blast simulations applying the DPM solver have successfully been verified by experiments [2], [3]. In this study, a model of the TARDEC Generic Vehicle Hull is used as the target structure where the soil model parameters are calibrated to match the experiments in [4]. Included within the Generic Vehicle Hull model is a seated IMPETUS Afea Hybrid III 50th Percentile Dummy to acquire occupant performance information.

Recent studies of fragmentation have shown a clear advantage when using a node splitting algorithm over the classic method of element erosion [5], [6], [7]. Simply, erosion does not capture fragmentation correctly as elements are removed during the simulation. Node splitting retains elemental mass to allow for the development of the fragments that ultimately impact the structure. A numerical study of fragmentation of a cylinder with respect to changes in element type, mesh size, number of HE particles, etc. is presented. This is done using a finite element model that represents the configuration given in [8], [9], [10] in order to compare with experimental results and a representative set-up. The knowledge gained with a simple cylinder will then be applied to modeling an artillery shell filled with HE and buried in soil. This concept model can then be used to determine the influence of the charge size on the total blast impulse acting on the Generic Vehicle Hull structure, as well as the dummy response.

SENSITIVITY STUDY OF FRAGMENTATION CYLINDER

To obtain knowledge of the fragmentation characterization inherent in the explosion of a cylinder and the numerical parameters involved in the process, replication of the experimental work of D. M. Goto [9], [10] is modeled. In the Goto experiment, cylinders and rings are filled with HE and detonated. Metal cylinder fragments are collected and measured to determine number and size. The experiment defines an AISI 1018 cylinder, 203.2mm in length, with an outside diameter of 50.8mm, and a thickness of 3mm. The HE used is LX-17 from Lawrence Livermore National Laboratory. For the given cylinder dimensions, the charge size is 0.648kg.

A base model is adapted and parameters are varied in order to observe the influence on number of fragments and fragment mass. For a quick evaluation, the total number of fragments from the simulations are compared. For a more in depth comparison, the accumulated mass versus fragment mass is compared, as well as the number of fragments versus fragment mass size. When the latter is compared to experiment, the interval for the fragment sorting according to mass size is done the same whenever possible. Experimental and numerical curve plots are in 1 gram intervals. Please note in the literature that although fragment recovery systems are used, 10% - 30% of the cylinder is not recovered [11].

The work carried out in this sensitivity study led to implementation of new functionality in the IMPETUS Afea Solver Engine and GUI. A file that lists the fragment information such as fragment ID, fragment mass, position, and velocity is written at the final simulation state. Also written is a file that shows the fragmentation distribution displayed in a plot of accumulated mass versus fragment mass. The IMPETUS Solver GUI has been updated to manage these files, making it easy to post-process results for fragmentation applications.

Base Model

The base model was adapted from [12] with very few changes and modeled with the IMPETUS Afea Solver® consistent with [7], [13], and [14]. The set-up is shown in Figure 1. The best description of the numerical model is found in [7].

Figure 1: *The set-up of the sensitivity model. A steel cylinder is filled with LX-17 HE.*

Reasonable agreement was found with the experiment presented in [15], [16] when considering mesh density. The response parameter considered was a plot of normalized number of fragments versus the fragment mass.

LX-17 is modeled using the discrete particle method (DPM) and with a user defined HE formulation. A total of

200,000 particles are used for the HE. The detonation point is located at the end of the top cone. The c_{dec} parameter is set to smear out gas-structure impulse in time to produce a smooth pressure signal.

The cylinder is modeled with ASET™ cubic elements. These elements are fully integrated and very accurate as a result of their 64 integration points. A total of 21,600 elements are used in the base model with 120 in the axial direction, 90 in the circumferential direction and 2 in the thickness direction, resulting in an aspect ratio close to 1 (element size in the range 1.5-1.7mm). The applied strength and damage model is similar to the Johnson-Cook formulation. However, due to the lack of material data, only D1 is specified with linear damage softening of the strength.

Randomly distributed initial damage is defined by *INITIAL_DAMAGE_RANDOM where a distribution function describes the number of defects per unit volume [17]. Other random distributions method could have been used as well. For example, random thickness could be employed to establish a geometric distribution defect. However, for the M795 artillery shell model it is assumed better to use the random damage function since the shell already has geometric variations. For model consistency from the cylindrical geometry to the shell, the random damage function was used here as well.

Modeling fragmentation with element erosion requires a very fine Lagrangian mesh since the mass is a key parameter together with the fragment size and velocity. To maintain the integrity of the mass balance (beginning total mass equals ending total mass), mass needs to be conserved in the simulation. In IMPETUS, a node splitting algorithm splits the higher order elements along the element edges and keeps the mass in the model.

In Figure 2, the evolution of the fragmentation progress in the simulation is seen at 10, 25 and 50µsec. It is seen that the expected cone shape of the expanding cylinder is obtained.

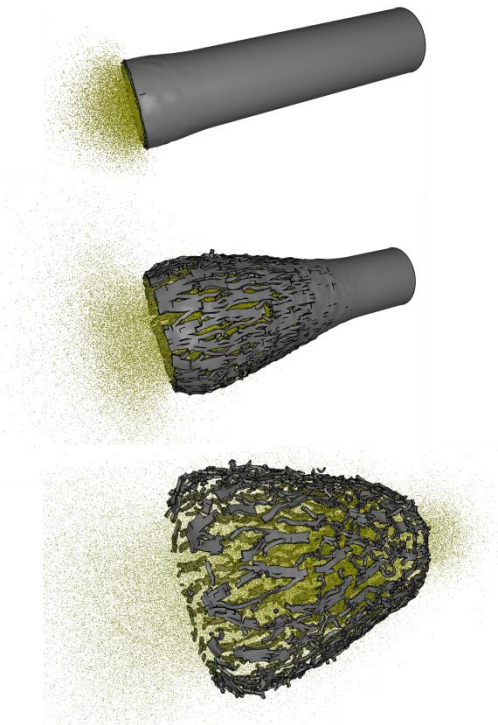

Figure 2: *The fragmentation of the cylinder at 10, 25 and 50µsec.*

In fragmentation analysis, the number of fragments and mass of each fragment is important as it provides information about the fragmentation process. In Figure 3, the normalized number of fragments is plotted against the fragment mass for both the base model and the experiment.

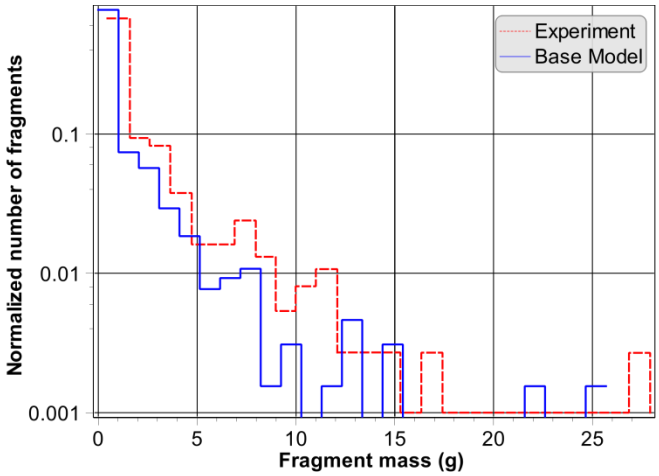

Figure 3: *Normalized number of fragments versus fragment mass for the base model and experimentally obtained data.*

It can be seen that the majority of the fragments are smaller fragments in fairly good agreement with experiments. The numerical curve of the base model will be higher given that not all the mass was recovered in the experiment as mentioned earlier. Please note that the fragmentation mass interval is kept the same in both curves.

In anticipation of fragment collisions, a contact algorithm between the fragments is also applied.

Figure 4 shows a magnified view of the structure depicting the mesh and HE particle interactions.

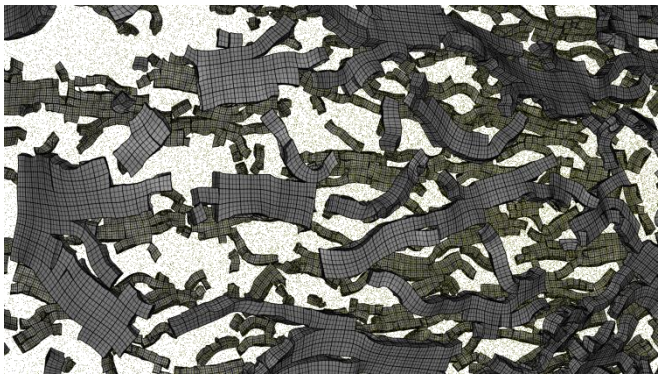

Figure 4: *There is specified contact between the fragments. A good element aspect ratio can be seen and the HE particles are also shown.*

The mesh illustrates that a good element aspect ratio is used, though in general that is not a requirement for the ASET™ Elements.

Given IMPETUS utilization of GPU parallelization technology, the computational time for the base model is less than one hour with a Nvidia K40 GPU accelerator.

Design Space

When developing a design space or an experimental matrix it is often difficult to decide which design variables have influence on the response parameters and their sensitivity. In this study the focus has been on numerical design variables. A total of nine design variables have been investigated, including the number of HE particles and mesh size. The values of the variables are selected within what is believed to be meaningful physical boundaries. The design space is built based on the following design variables that are described in more detail in the next section:

- General: number of HE particles.
- Mesh: number, order and type of elements.
- Material: random damage, type of node splitting.
- Blast: smearing of impulse.

Numerical Results from Sensitivity Study

The simulations were run on various hardware platforms, but all included the NVIDIA K40 GPU for parallel processing. The same version of the solver was used for all simulations.

When using the discrete particle method, the total number of particles has to be specified. In this case soil and air particles are omitted, thereby allocating all particles as HE particles. In [18] it is shown that the method converges when increasing the number of particles of the soil in a buried mine blast event with the blast impulse as the response parameter. The number of HE particles was varied between 100,000 to 1,000,000 particles and the total number of fragments is counted. Figure 5 shows that for 400,000 particles, the method converges. It should be noted that the number of fragments is for the mesh of the base model, which is considered coarse when counting the number of fragments. The convergence provides confidence in the implementation of the DPM.

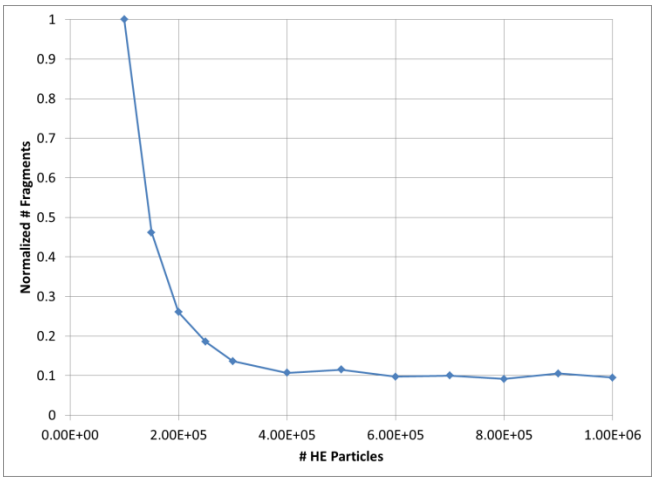

Figure 5: *The DPM in IMPETUS convergences with regards to number of HE particles.*

Interestingly, when defining the numerical model with fewer particles, each particle has a greater share of the total particle mass. This results in a larger localized impulse and more severe impact. This in turn creates more fragmentation as can be observed in Figure 5. Based on the graph, the number of particles recommended for this mesh is at least 400,000, but one should look at the particle size compared to the element size. The particle radius can be found in the

impetus.info file and it is 0.546mm for the base model with a mesh length of approximately 1.7mm. This gives a ratio of 3. For the 400,000 particle model, the HE particle radius is 0.433mm and the mesh size is the same. Thus, the ratio is 4 which then is recommended as a minimum. It may also be relevant to investigate the mass ratio, but this is left for future work. For the models with a large impulse due to fewer particles, elements are eroded because of very small time step. As discussed earlier eroded mass from the simulation is not advisable for modeling fragmentation, or at least it should be at a minimum. The accumulated fragmentation mass as a function of the fragmentation mass can be plotted from the output files and then compared with the physical mass. This will indicate if mass is conserved in the simulation or if there is a loss of mass. This is shown in Figure 6 for the base model (200,000) for 100,000, 400,000 and 1,000,000 particle models. Figure 6 shows the base model has approximately 3.78% mass loss.

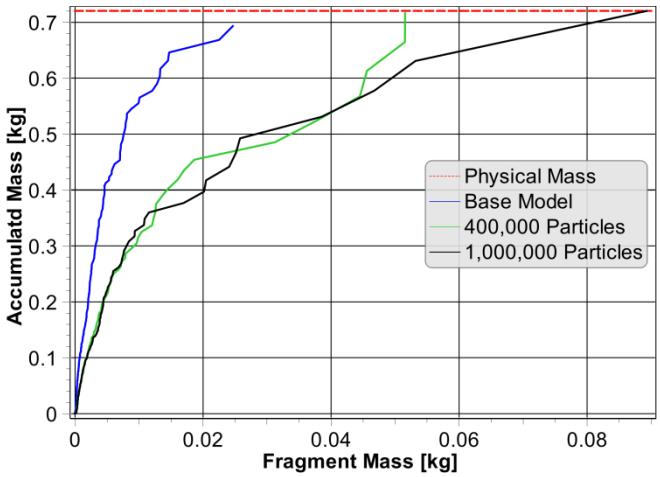

Figure 6: *Accumulated mass as function of the fragmentation mass. It can be seen that the base model has a mass loss, whereas this is not the case for the 400,000 and 1,000,000 particle models.*

The base model mesh consists of 21,600 cubic hexahedron elements. A mesh sensitivity study was conducted comparing 10 different mesh densities, with the finest mesh being 72,900 elements. The number of elements in the thickness direction was tested for 2, 3, and 4 elements. In Table 1, the different mesh densities are provided.

Mesh	Base	Exp. 1	Exp. 2	Exp. 3	Exp. 4	Exp. 5
Thick	2	2	2	2	2	2
Circ.	90	99	113	135	145	150
Axial	120	132	150	180	190	200
Total	21600	26136	33900	48600	55100	60000
Mesh	**Exp. 6**	**Exp. 7**	**Exp. 8**	**Exp. 9**	**Exp. 10**	
Thick	2	2	3	3	4	
Circ.	160	160	90	135	90	
Axial	200	220	120	180	120	
Total	64000	70400	32400	72900	43200	

Table 1: *Investigated mesh densities. Numbers of elements in the thickness directions as well as circumferential and axial directions are varied. All elements are cubic hexahedron elements.*

It was observed that increasing the mesh density led to an increase of fragments. With only a ductile failure criterion activated, the energy required to drive the crack becomes mesh dependent. The finer mesh, the less energy is needed. This problem can be circumvented with a complementing fracture energy criterion. In fact, the IMPETUS Afea Solver® has a fracture energy criterion implemented. The energy to drive the crack growth then becomes mesh insensitive. However, having no real material data at hand for this study, it was decided to keep things as simple as possible. It is to be noted that the ductile failure criterion is used to predict crack initiation while the fracture energy criterion is used to predict the crack growth. Having the fracture energy criterion activated generally makes the cracking propagation process more brittle, at least for coarse meshes. Hence, it seems reasonable to believe that the real base material is more ductile than assumed in this work. This would explain why the finer meshes predict too many fragments

It was discovered that the number of fragments was somewhat linear depending on the mesh size. The results for the smallest (Exp. 1) and largest mesh (Exp. 9) for two elements through the thickness are shown in Figure 7, where the base model and experiments are plotted.

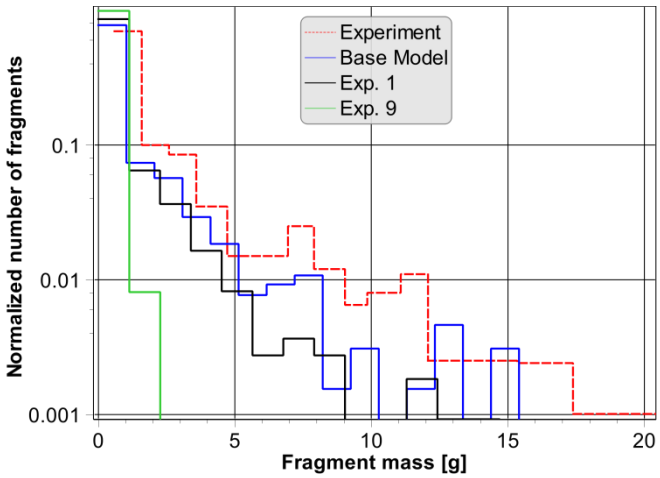

Figure 7: *Influence from the mesh density on the normalized number of fragments. Shown is experiment 1 and 9 together with the base model and experimental results.*

Experiments 8 and 10 have different number of elements in the thickness direction but the same mesh size in the axial and circumferential directions. The number of elements is 3 and 4, respectively. The base model has two in the thickness with the same mesh size. It can be seen that more elements lead to more fragments and that the results for 2 and 3 elements in the thickness are similar as shown in Figure 8.

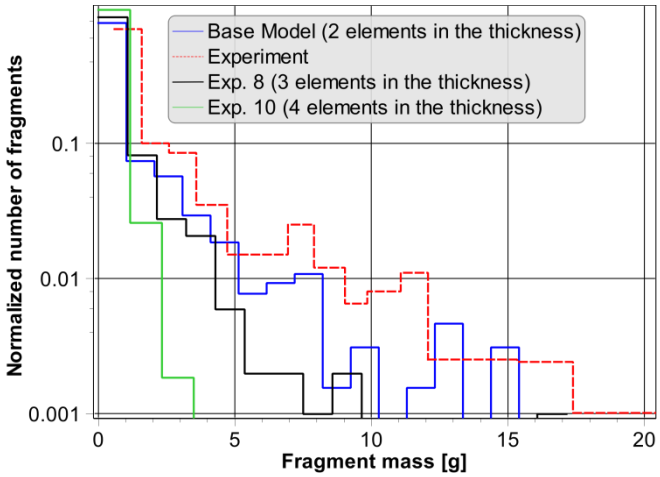

Figure 8: *Normalized number of fragments based on the number of elements in the thickness direction of the test cylinder.*

The ASET™ family of higher order elements includes linear, quadratic and cubic elements, with the latter being the "work horse" element. It is simple to change between the different orders of the element since only the order parameter on *CHANGE_P-ORDER needs to be specified to 2 or 3 for quadratic or cubic elements, respectively. This can be done for the whole model, a part or even only within a region. The base model has been tested with linear, quadratic and cubic elements for the same mesh size. Furthermore, a model was created with a mesh that had linear elements and was three times larger in all directions to compare with the cubic elements. However, a comparison is not direct since the piecewise linear distribution for the linear elements is not the same as the polynomial distribution obtained in the cubic element. The linear mesh should be further tested with an increased number of elements so that the node spacing matches the node spacing used in the cubic element model.

The linear model resulted in approximately one third of the number of fragments obtained in the base model. A large number of fragments were seen for the dense linear model and many elements were eroded due to a small time step. This is due to the fact that the linear elements are unable to deform to the same magnitude as quadratic and cubic elements.

Figure 9 shows a graph of the number of fragments versus the fragment mass for the quadratic and cubic elements together with the experimental results. The quadratic element model has a few larger segments that are not observed in the experiment. The results get closer to the experiment for smaller fragments, though it should be recalled that not all fragments were found in the experiments. It could be argued that these missing fragments are smaller fragments that would raise the first part of the curve closer to the cubic element model. Based on this and the observed larger fragments for the quadratic elements, it suggests that to obtain more accuracy one needs to use cubic elements.

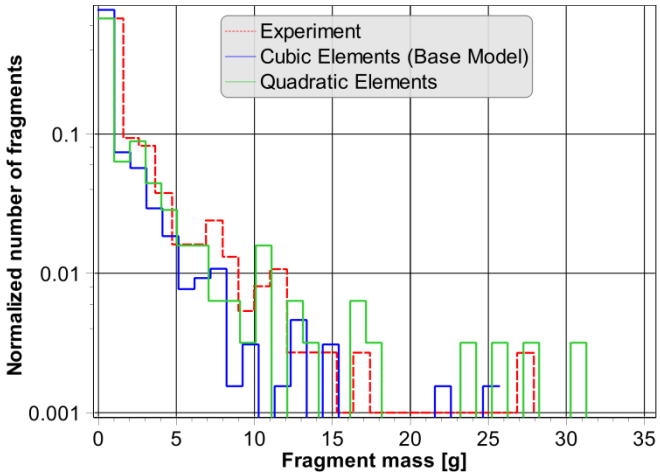

Figure 9: *Comparison of the normalized number of fragments versus mass for experiments, quadratic and cubic elements.*

A series of tetrahedron based meshes were also developed and tested. It would be very beneficial if tetrahedron elements could be used since it will allow for automeshing. Furthermore, a tetrahedron mesh gives rise to more possible fragmentation paths than a hexahedron mesh which can be beneficial for fragmentation modeling. Four different mesh configurations were tried, all a multiple of the number of elements in the base model. The meshes are 1, 2, 3, and 4 times the number of elements in the base model, thus the largest tetrahedron model (quadrupled mesh) consists of 86,074 elements. Roughly a multiple of the hex mesh, the slight difference has an insignificant effect on the results. The results are shown in Figure 10, where the number of fragments increases with the number of elements. Note this was also the case for hexahedron elements, though the tendency is less for the tetrahedron elements.

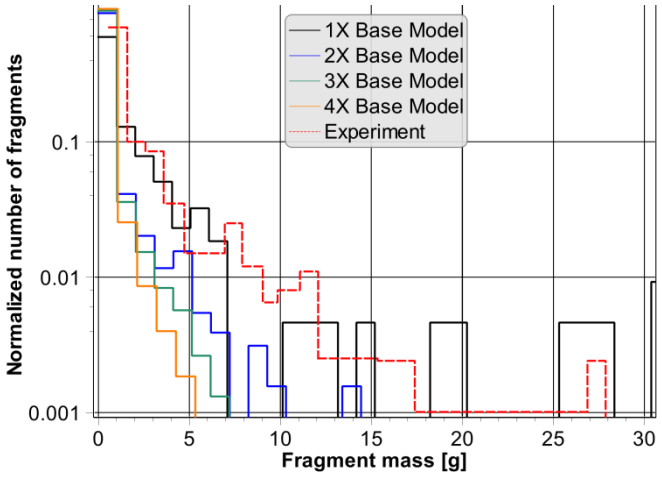

Figure 10: *Results of the simulations with tetrahedron meshes. Normalized number of fragments as function of fragment mass.*

Random Damage

No real material is perfectly homogeneous. There are always weak spots (defects) where the cracks tend to initiate. The defect severity and distribution will affect the resulting fragmentation distribution. In finite element modeling of the process, the cracking will follow the mesh lines when node splitting is applied. This is not representative of the real behavior. To take the defects into account, initial damage of the material can be included. In IMPETUS this is done with the command *INITIAL_DAMAGE_RANDOM, where a distribution function is applied to describe the number of defects. This function is given by:

$$f(D) = \begin{cases} ae^{-bD} & D \leq D_{max} \\ 0 & D > D_{max} \end{cases}$$

where a and b are constants to be specified by the user and D_{max} is the maximum allowed initial damage. The number of defects, N, per unit volume is found by integration of $f(D)$ over the damage range D_0 to D_{max}, leading to:

$$N = \int_{D_0}^{D_{max}} f(D)dD$$

The probability p of having at least one initial defect that is larger or equal to D_0 in volume v is [17]:

$$p = 1 - e^{-Nv}$$

Knowing the volume v and generating a random number p, the initial damage D_0 can be calculated. The initial damage is applied at each integration point. It should be mentioned that if the same run is repeated, the results will be the same, because IMPETUS uses the same random number, making the run repeatable. It is expected that defining the initial damage will have a significant influence on the results. As mentioned the values in the base model are taken from [12], but in [13] it was mentioned that the values have been found from curve fitting of results from a large number of tensile tests. Several combinations of values have been tested, though a combination of changing more than one variable at a time has not been carried out. This is left for future work. The different test settings are shown in Table 2. The numbers in bold are the values tested. Experiment 1 (Exp. 1) is the base model and Exp. 2 is a model where no initial damage is given.

Exp. #	a	b	D_{max}
1	1e+9	7.45	0.7
2	**0.**	**0.**	**0.**
3	**1e+11**	7.45	0.7
4	**1e+3**	7.45	0.7
5	1e+9	**1.5**	0.7
6	1e+9	**12**	0.7
7	1e+9	7.45	**0.4**
8	1e+9	7.45	**0.9**

Table 2: *The different combinations for applying random initial damage to the structure. The values in bold are settings different from the base model.*

To compare the combinations directly with a single response parameter, the total number of fragments were counted for each model and normalized with the count from the base model. Based on the equations, it is expected that

increasing the value of *a* will result in more fragments. This is also assumed to be the case if D_{max} is increased. However, when *b* is increased in value, the exponential function gives a smaller value due to the negative sign in the equation leading to less initial damage and hence, it is expected that the number of fragments will be smaller. The results of the numerical models are plotted in Figure 11, where it is seen that Exp. 1 is significantly different than the results from the base model. The *a* parameter was set to a much higher value than applied to the base model. The other parameter that strongly influences the behavior is Exp. 5, which lowered the value of *b* to 1.5, compared to 7.45 used in the base model. The results also indicate that the use of no initial damage actually generates results close to the base model. This is also the case with the rest of the parameters. This could be due to too small a variation in the parameters, such that the changes are not aggressive enough to provoke changes in the number of fragments. It should be remembered that this is the final count of fragments, not the distribution.

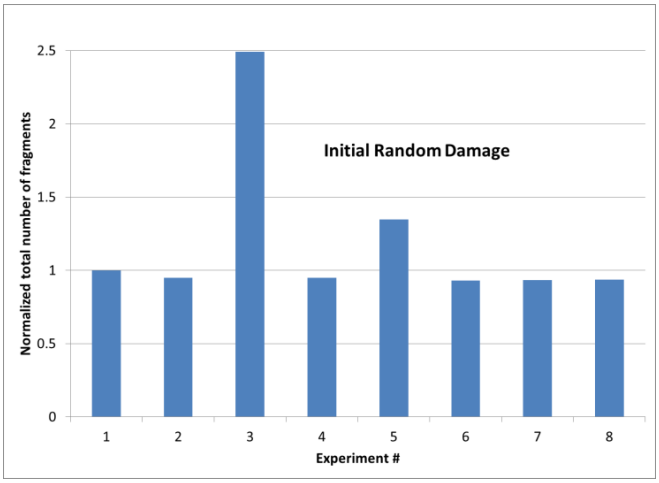

Figure 11: *Normalized total number of fragments depending on the setting for the random initial damage. The setting for each experiment is listed in Table 2. The number of fragments is normalized with regards to the base model results.*

To further investigate the results for the simulations where significant changes are obtained, the normalized number of fragments as function of the fragment mass has been plotted for the baseline, no initial damage, *a*=1e+11 (Exp. 3), and *b*=1.5 (Exp. 5). These plots are shown in Figure 12.

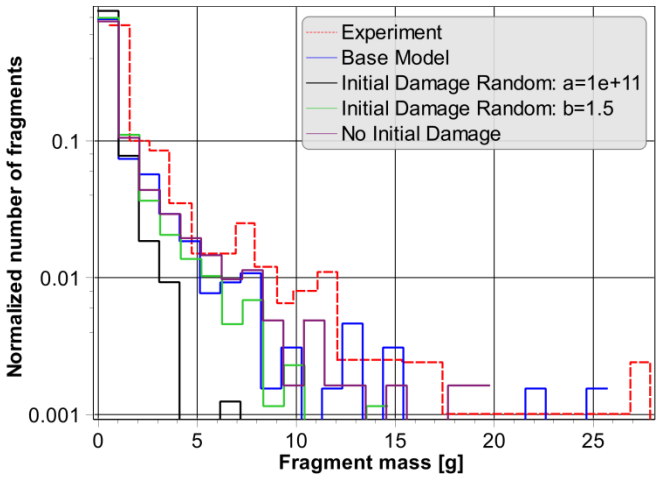

Figure 12: *Normalized number of fragments versus fragment mass for the base model, experimentally obtained data, no initial damage, Exp. 3 and Exp. 5.*

Notice that the setting of the *a* parameter can have a large influence on the results. The plots also show that the values applied for the base model seem reasonable when compared to the other values that were tested. However, it is suggests that more in-depth research should be carried out to investigate the influence of initial random damage.

Node Splitting Algorithm

When full damage in the material is reached, different options are available. Options include the element remaining intact, it can erode, or node splitting along the element edge may be invoked. The later causes a crack plane to be created along which the nodes are split and new surfaces are created. The direction of the plane is specified as input. The node splitting algorithm has two options for the orientation of the crack plane normal. The crack plane may be orthogonal to the maximum principal strain, or it may be orthogonal to the principal stress. This is *erode*=2 and *erode*=3, respectively and defined with the *PROP_DAMAGE_*option* command. If spalling occurs in the model, then *erode*=2 should be used, but if not, there is not a large difference between the two options. Option 2 has been seen to produce less noise in the response since the maximum principal strain tends to be more stable in time than the maximum principal stress. The base model uses both *erode*=3 and *erode*=2 for comparison.

Plots of the normalized number of fragments versus the fragment mass are compared in Figure 13, where the abscissa is cut at 20 gram to increase visibility. For *erode*=2 there were larger fragments. A large difference was not observed, which could indicate that not much spalling has occurred. If one of the options should be selected, *erode*=3 is preferred.

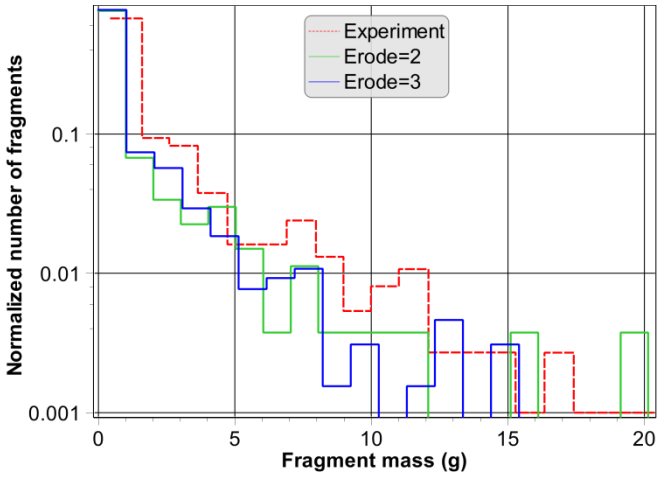

Figure 13: *Comparing the two different options for setting the node splitting algorithm with experiments.*

Blast Smearing Impulse.

In models where the HE is confined in a container it can be beneficial to smear out the impulse in time. This will give smoother pressure load from the HE particles. In the *PBLAST command, the c_{dec} parameter gives the option to do this. The impulse from one impact is smeared out in time with an exponential decay function. If i is the discrete impulse at time t, then the pressure p at $t_1 > t$ from that specific impact becomes:

$$p(t_1) = \frac{i}{Ac_{dec}} e^{\left(\frac{-(t_1-t)}{c_{dec}}\right)}$$

where A is the element face area where the pressure is applied.

However, it will only have a significant smoothing effect if c_{dec} is larger than the element time step size. Otherwise the element will behave as if the load is more or less instantaneous. In the base model, the element time step is $\Delta t_{element}$ = 0.15e-6 so it seems reasonable to specify c_{dec} as 1.0e-6 as done in the base model.

Four different settings of the c_{dec} parameter were tested: No c_{dec}, 1e-7, 1e-6, and 5e-6. In the base model, c_{dec} was specified as 1e-6. If c_{dec} is not used, or is set as low as 1e-7, it will generate higher peak impulses and lead to more and smaller fragments. This was observed and is shown in the data. These two cases have approximately 7 times more fragments than the base model. The number of fragments versus fragment mass curves are plotted in Figure 14. It is observed that setting the c_{dec} to 5e-6 yields results that are closer to the experiments than the base model when looking at the first group of fragments. The results also indicate that the selection of this parameter is very sensitive, but should be used in fragmentation modeling. It could be that the parameter would be less significant if more HE particles were used since that would smooth out the pressure as well. More tests and research should be done regarding this parameter.

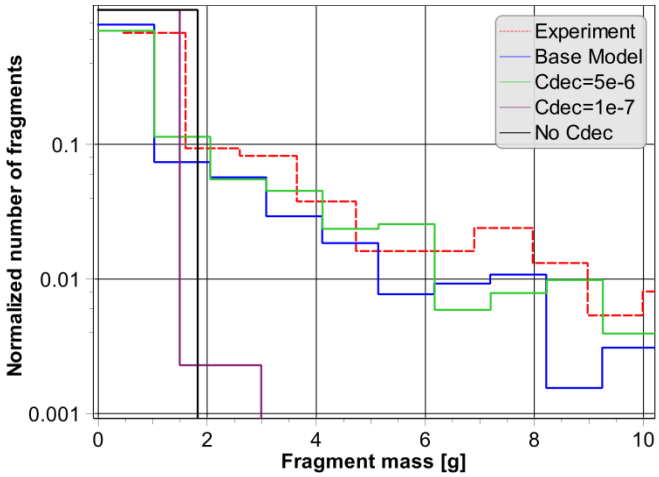

Figure 14: *Sensitivity of changing values of the c_{dec} parameter on the *PBLAST command. The plots show normalized number of fragments versus fragment mass.*

MODELING ARTILLERY SHELL AS IED

The 155mm M795 HE artillery shell was chosen as the IED. It has 10.8kg TNT, a total mass of ~ 46.7kg, and a length of approximately 0.84m. The charge size of 10.8kg exceeds a STANAG 4569 Level 4 threat by 0.8kg [19]. Smaller charges could also have been used and it would be interesting in the future to test the response from different charge sizes.

The casing is made out of HF1, high fragmentation steel. Open source literature for the dimensions of this artillery shell is limited. Hence, an approximation to the real geometry was made based on the constraints of the total mass, TNT mass, and overall dimensions which were found partly in [20-23]. The model is shown in Figure 15, where the HE also is included.

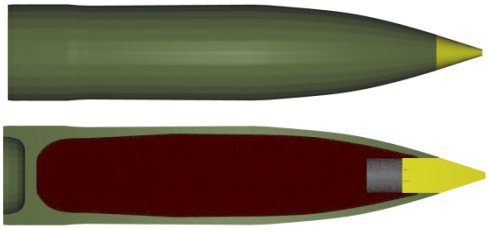

Figure 15: *Modeling the 155mm M795 artillery shell.*

In the first model, the casing consists of 5640 cubic hexahedron elements, where the sidewalls have two elements through the thickness. Figure 16 shows a section cut of the shell to illustrate the applied mesh.

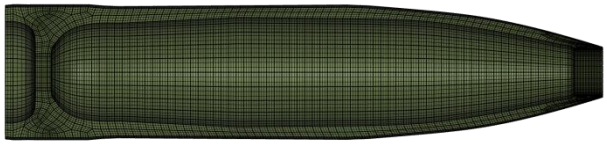

Figure 16: *Mesh applied for the M795 artillery shell. Only half of the model is shown for visibility. The meshing was done by IMPETUS AB, Sweden.*

As with the dimensions, finding material data for the HF1 steel was difficult as no open source literature documents revealed damage parameters for the Johnson-Cook damage model or other criteria. The material parameters found in different publications were compared [24-32]. As these are rather old references and characterize the model as bi-linear plasticity with maximum elongation, it was decided to use the Johnson-Cook strength model with the values listed in [32]. This model includes thermal softening and strain rates. The damage is done with the Cockcroft-Latham criteria [33], setting W_c=750 MPa. The value is found from studying the fragmentation behavior for different settings of W_c and then choosing which value seems reasonable. Furthermore, a fracture energy parameter, G_I, is added which makes it possible to model crack propagation. It also makes the fragmentation less mesh dependent as mentioned in the description of the sensitivity study. The value is selected based on the authors experience with this option. Based on the knowledge from the base model, linear damage softening is used to couple damage to the strength model. In the initial model of the M795 shell node splitting was invoked by setting *erode*=3 and initial random damage was applied the same as for the base model. However, these values resulted in a very brittle response leading to a change in parameters, mainly lowering the value of *a* from 1e-9 to 1e-7. Both the fuse parts are modeled as rigid, assuming that their influence on the explosive behavior is minimal. This assumption can be tested in the future.

The first model of the M795 included the HE, shell, and the fuse parts. This was done to get familiar with the response of the model under the severe loading from the HE. A total of 100,000 HE particles were used; a number that could change for the total model that includes soil, hull and dummy as a total number of particles is specified with the *PBLAST command. IMPETUS will automatically distribute the particles between the HE, soil and air domains. Normally, air is not included for buried mine blast events [2] and [18]. The impulse is smeared according to the findings for the base model so c_{dec} is set to 5e-6. The termination time was set at 150μsec.

The goal was to develop a "total model," which includes the M795 artillery shell with TNT, buried in soil, and detonated impacting a structure. The depth of burial (DOB) was selected as 4 inches. The TARDEC Generic Vehicle Hull model was placed above the soil with a stand-off distance of 17 inches, included in the hull model was the IMPETUS Hybrid III 50th Percentile Dummy model in a seated position. The dummy model was chosen according to the guidelines of [34].

The development of the total model was done in three stages. Stage 1 the artillery shell and the HE were modeled. Stage 2 consisted of stage 1 plus soil. Finally, stage 3 consisted of stage 2 plus the hull and the dummy. Figure 17 highlights the various stages, where the shell and the HE are the main focus in stage I.

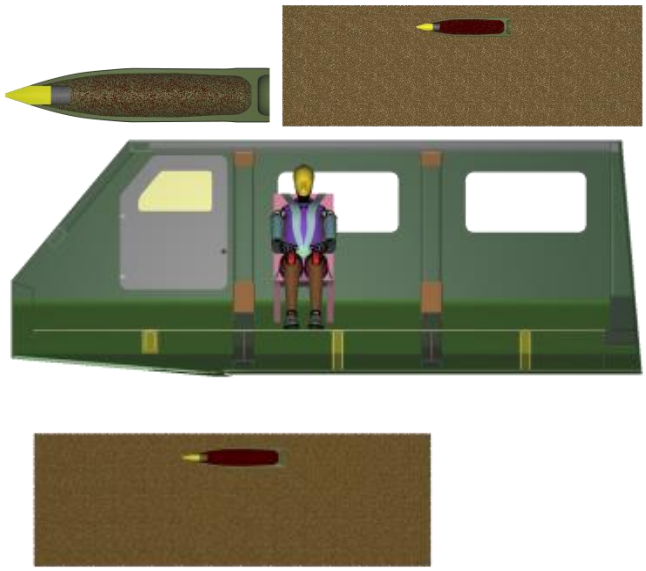

Figure 17: *Development of the fragmentation process for the M795 artillery shell. Note, half models are shown to have a better view of the setup. The process of developing the total model was divided into three stages. The final model includes M795, HE, soil, hull and the dummy.*

The stage I model uses hexahedron elements, which exhibit fragment lines along the mesh lines. However, there are asymmetric fragment patterns due to the random damage (vertical cracks). A finer mesh one would assume would give more randomness but at an added computational cost. The results at times 50, 100 and 150μsec are shown in Figure 18.

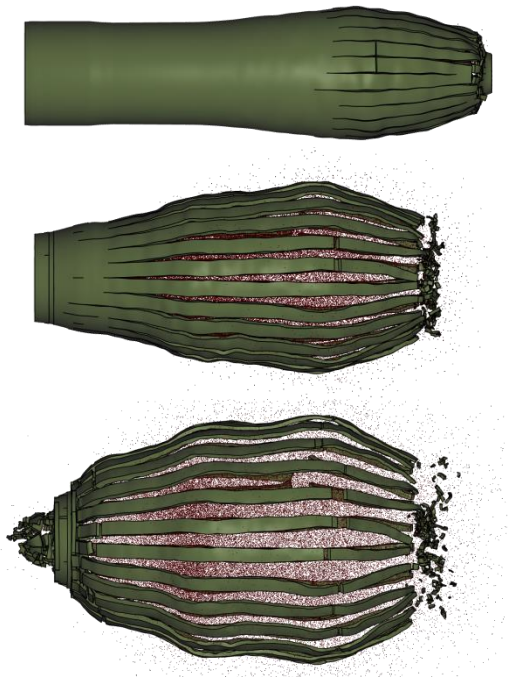

Figure 18: *Development of the fragmentation for the M795 artillery shell at times 50, 100 and 150µsec, using cubic hexahedron elements.*

As mentioned in the sensitivity study, tetrahedron elements generate more random mesh lines and hence would lead to a more random fragmentation path. To investigate the use of tetrahedron elements a new mesh for the casing was created, consisting of 7,159 cubic tetrahedron elements.

Figure 19 shows the results for the tetrahedron model for various times in the simulation. It is seen that fragmentation is non-symmetric.

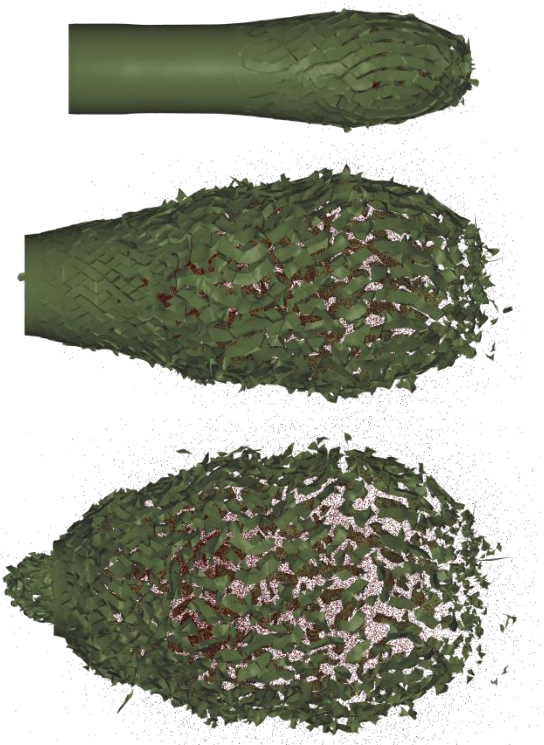

Figure 19: *Fragmentation for the model using tetrahedron elements at time 50, 100 and 150µsec.*

Although there is no experimental data to compare with, the results seem reasonable. The size and amount of the fragments may change by specifying a different value for the *a* parameter and the damage value, but experimental data would be needed. A zoom of the model results at time 150μsec is shown in Figure 20 where it can be seen that the fragments are non-uniform and exhibit a non-symmetric distribution.

Figure 20: *Fragments for the model using tetrahedron elements. Notice the difference in the fragment shapes and size.*

The M795 model is included in the stage 2 model, where the shell is buried in soil. Including the soil means that the number of DPM particles specified is divided between the HE and the soil. A total of 8 million particles are used to obtain a certain number of HE particles which in this case is 58,952. For comparison, 4 million particles were used in [18] for a similar set-up, but only included modeling the HE and the soil, i.e., without the structure of the casing. As for the base model, a convergence study could be done, but this number of particles is believed to be enough to illustrate the concept and the trend.

The soil is defined with a user defined soil that represents the soil bed listed in [4], and the values are taken from the calibration done in [35].

Typically, the time for buried mine blast simulations is on the order of milliseconds and not microseconds as has been used for the fragmentation tests shown so far. From initial testing of the total model, it was observed that the fragments impact the hull structure at around 0.8msec. Hence, for the stage 2 model, a termination time of 1msec is used.

An observation for the initial test of the model was that the HE did not follow the structure of the shell. A gap was formed between the structure and the HE. When using the DPM for the soil there is an optimized internal contact algorithm that handles the contact between the soil and the structure. It is not necessary to give a contact between the soil and the structure, all values in this penalty formulated contact are calculated by the Solver. The authors have over the years been running hundreds of buried mine blast simulations and there has never been a failure of this contact. However, these simulations have been done with the traditional approach where no casing is used for the charge, thus no structure has been in contact with the HE or the soil under the initial detonation.

The *PBLAST command was recently updated to include a stiffness parameter, *pfac*, which was implemented for warhead simulations. Setting *pfac*=1e+13 made the contact behave as expected. However, the option seems to add computational costs so it should only be used when necessary. In order to keep the time step at an acceptable level, erosion due to time step and extreme strain has been applied to the model. Running the model for longer in stage 2, combined with the soil interaction, resulted in too many elements eroding for the coarse mesh. In response, the mesh density was increased and the model used 18,367 cubic tetrahedron elements for the shell. Figure 21 documents the development of the explosion at 0.12, 0.5, and 1.0msec to show how the HE and artillery shell fragments move with the soil. The mix of soil and HE particles can be seen as well as the interaction with the fragments.

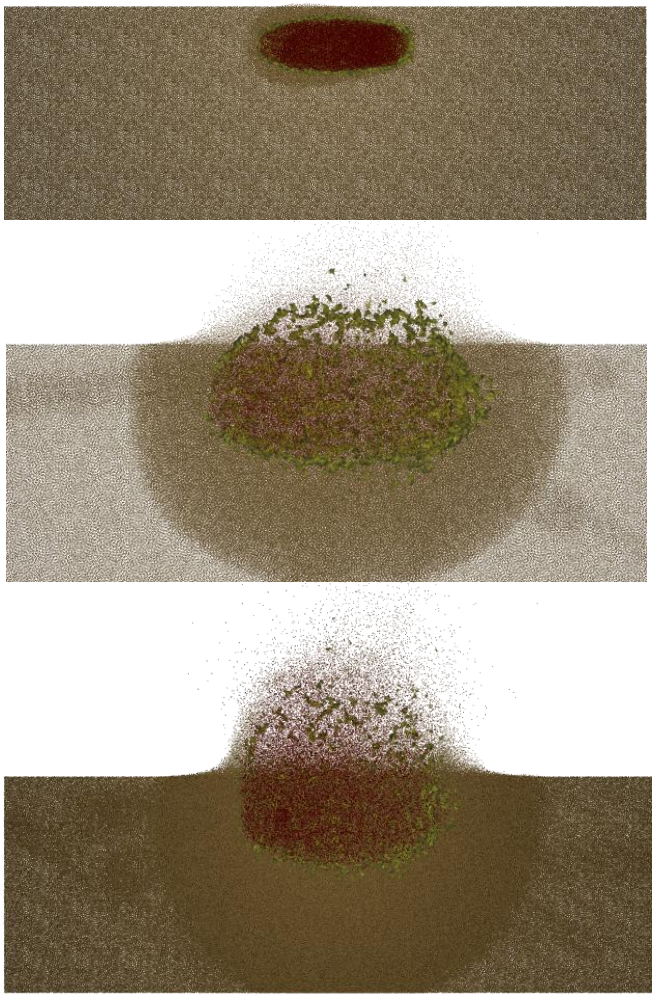

Figure 21: *M795 fragmentation in soil. The HE (red) impacts the artillery shell (green) to create the fragments. Soil (light brown) is moved by both the shell fragments and the HE. Results at 0.12, 0.5, and 1.0msec. Only half model is shown. The mixing of HE, soil and structural fragments can also be seen.*

To represent a complete scenario the TARDEC Generic Vehicle Hull and the IMPETUS Afea Hybrid III 50th Percentile Dummy is added to the model. The modeling of the M795 and the soil is kept the same. It was assumed that the influence of the artillery shell structure and fragments for the given under belly blast occur during the detonation and motion of the soil including the initial impact with the structure. This means that a difference should be noticeable during that timeframe. Based on that assumption, the termination time for the total model was set to 3msec. If desired, this can always be extended by the use of an advanced restart. The impact with the hull at 1 and 3msec is shown in Figure 22.

The mix of fragments, HE and soil particles can be seen. It can also be seen that the hull is largely deformed, causing the floor to breach.

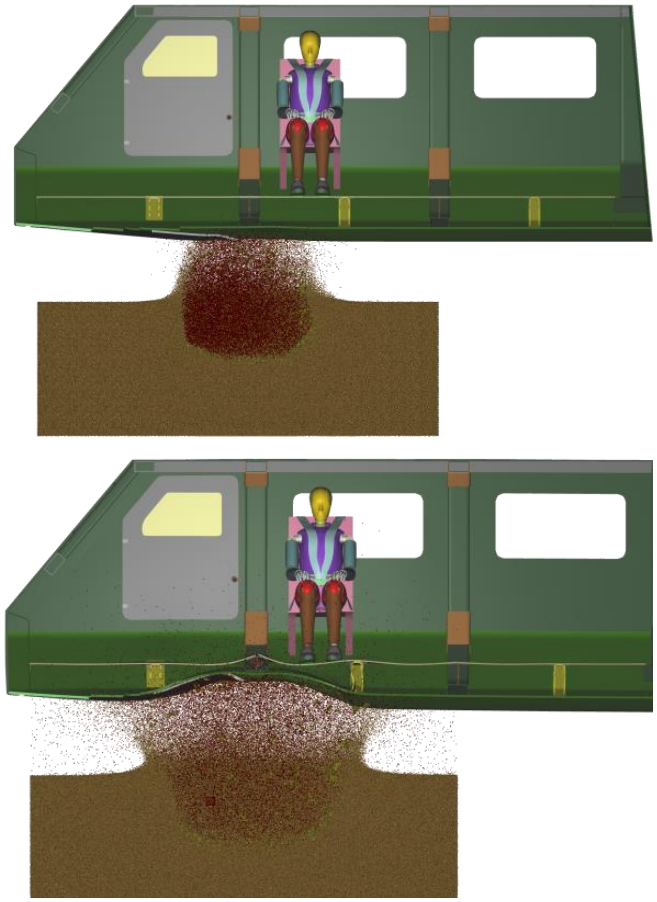

Figure 22: *The complete model including M795, HE, soil, hull and dummy. The interaction between the particles and the structural parts is observed and results in a large deformation of the hull. Only half model is shown.*

The fragments from the artillery shell are in contact with the bottom of the hull as illustrated in Figure 23. It was seen in all the M795 models that the main part of the computational time is spent in the contact update. The self-contact specified for the artillery shell fragments is a very difficult contact and increases in complexity and computational costs as more contact surfaces is generated through the fragmentation process.

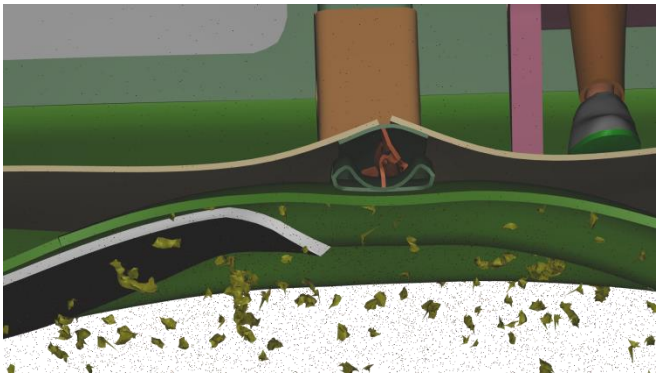

Figure 23: *Contact between the fragments and the bottom of the hull. Only half model is shown.*

The total model results appear reasonable and are promising for future studies of this complicated event. As mentioned, no material data could be obtained for the HF1 material so the fragmentation behavior could indeed be very different, but the framework is in place.

An important parameter for the mine blast event is the blast impulse on the structure. This is shown for the M795 and the hull in Figure 24. It was shown that the shell experiences the largest impulse during the initial detonation, whereas the impulse on the hull is delayed until the soil impacts it. This supports the decision made to only run the simulation for 3msec. However, if fragmentation impact on the occupant (dummy) is investigated, the simulation time will need to be extended. The ratio between the two impulses could be different when applying accurate material data for the HF1 steel.

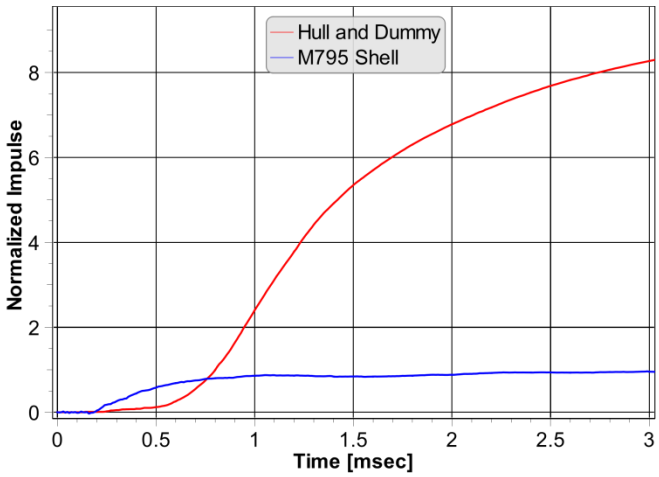

Figure 24: *Normalized total blast impulse in Z-direction for the hull and the M795 shell.*

CONCLUSION

The results of this paper conclusively show that it is feasible to simulate the blast and fragmentation of a HE filled, M795 artillery shell IED buried in soil, and the subsequent ejecta impact on the TARDEC Generic Vehicle Hull containing a seated IMPETUS Afea Hybrid III dummy using the explicit non-linear transient finite element software, the IMPETUS Afea Solver®.

Importantly, the authors believe that this paper provides modeling techniques to evaluate the blast and fragmentation effects of complex shaped IED's on a myriad of structures. While demonstrating multiple, plausible fragmentation outcomes, the authors are convinced that with improved HF1 material characterization and follow on live fire testing to clearly identify the material fracture and crack propagation processes that take place in shell casings during a blast, the most robust combinations of model and material parameters can be employed to achieve ever greater levels of event correlation. Ultimately, the learnings from these studies will lead to blast and fragmentation mitigating structures better able to protect military and civilian personnel from harm.

ACKNOWLEDGEMENT

"Many unclassified studies from past researchers have utilized fictitious vehicle geometry due to the non-availability of realistic information. Due to the sensitive nature of the work performed by the Department of Defense, data generated from testing military vehicles is usually classified, making it difficult to share data in the public domain. In order to increase the operational relevance of studies performed by the wider scientific community, the US Army Tank Automotive Research, Development and Engineering Center (RDECOM-TARDEC) has fabricated a generic vehicle hull to help evaluate blast mitigation technologies, and also shared an FEA model of the same for purposes of this research." It was necessary to develop a new model for the IMPETUS Afea Solver® and the authors would like to thank TARDEC, in particular, Dr. Ravi Thyagarajan, Mr. Madan Vunnam, and Dr. Bijan Shahidi for supporting the effort to develop the model.

The IMPETUS model of the fragmentation cylinder used for the sensitivity study was provided by Dr. Jérôme Limido and Mr. Anthony Collé, IMPETUS Afea SAS, France. Further, the authors would like to thank Dr. Limido for the many helpful discussions.

Eric Lee, IMPETUS AB, Sweden created the FE model of the M795 artillery shell based on very crude dimensions and other limited information available in the public domain. The authors are thankful for his assistance.

David M. Gerst, Navistar Defense, is gratefully acknowledged for sharing literature and for general discussions regarding fragmentation.

REFERENCES

[1] T. Zeleznik et. al., "Analysis of Craters from Large Buried Charges", 2015 NDIA Ground Vehicle Systems Engineering and Technology Symposium, August 4-6, 2015, Novi, Michigan, USA.

[2] W. L. Mindle et. al., "The Discrete Particle Approach to Modeling Air, Soil and HE for Blast Simulations", 2014 NDIA Ground Vehicle Systems Engineering and Technology Symposium, August 12-14, 2014, Novi, Michigan, USA.

[3] T. Børvik, L. Olovsson, A. G. Hanssen, K. P. Dharmasena, H. Hansson and H. N. G. Wadley, "A Discrete Particle Approach to Simulate the Combined Effect of Blast and Sand Impact Loading of Steel Plates", Journal of the Mechanics and Physics of Solids 59 (2011) 940-958.

[4] K. Williams et. al., "A Numerical Analysis of Mine Blast Effects on Simplified Target Geometries: Validation of Loading Models", Report No. DRDC-VALCARTIER-TM-2002-260 (2003).

[5] J. F. Moxnes et. al., "Experimental and Numerical Study of the Fragmentation of Expanding Warhead Casings by Using Different Numerical Codes and Solution Techniques", Defence Technology 10 (2014) 161-176.

[6] J. K Holmen et. al., "Influence of Fragmentation on the Capacity of Aluminum Alloy Plates Subjected to Ballistic Impact", Journal of the Mechanics A/Solids 55 (2016) 221-233.

[7] A. Collé et. al., "Innovative Lagrangian Numerical Approach for Natural Fragmentation Modeling", 29th International Symposium on Ballistics, Edinburgh, Scotland, UK, May 9-13, 2016, 1590-1601.

[8] D. M. Goto et. al., "Investigation of the Fracture and Fragmentation of Explosive Driven Rings and Cylinders", LLNL Report, UCRL-JRNL-230155, 2007.

[9] D. M. Goto et. al., "Explosive Driven Fracture and Fragmentation of Metal Cylinders and Rings", LLNL Report, UCRL-CONF-230236, 2007.

[10] D. M. Goto et. al., "Investigation of the Fracture and Fragmentation of Explosive Driven Rings and Cylinders", Journal of the Impact Engineering 35 (2008) 1547-1556.

[11] C. W. Arthur et. al., "Investigation of the Fragmentation of an Explosively Driven Cylinder", LLNL Report, LLNL-TR-666136, 2015.

[12] Dr. Jérôme Limido, CTO, IMPETUS Afea SAS, France, Private Communication.

[13] A. Collé, "Monolithic Lagrangian Approach for Warhead Natural Fragmentation Modeling", Master Thesis, ISAE-ENSMA, France, September 2015.

[14] L. Olovsson et. al., "Modeling Fragmentation with new High Order Finite Element Technology and Node Splitting", DYMAT 2015, EPJ Web of Conferences 94, 04050 (2015).

[15] F. Caleyron et. al., "A Meshless Method for Fluid-Structure Interactions: Application to the Failure Prediction of a Tank Under Impact", COMPDYN 2011, ECCOMAS Thematic Conference on Computational Methods in Structural Dynamics and Earthquake Engineering, Corfu, Greece, 25-28 May, 2011.

[16] J. M. Owen, "ASPH Modeling of Material Damage and Failure", LLNL Report, LLNL-PROC-430616, 2010.

[17] The IMPETUS Afea Solver Online Manual: http://www.impetus-afea.com/support/manual/

[18] M. R. Jensen et. al., "Discrete Particle Method is a Predictive Tool for Simulation of Mine Blast – A Parameter Study of the Process and Approach", Proceedings of the 2015 NDIA Ground Vehicle Systems Engineering and Technology Symposium (GVSETS), August 4-6, 2015, Novi, Michigan.

[19] NATO Standardization Agency, "STANAG 4569 (Edition 2) – Protection Levels for Occupants of Armoured Vehicles", 18/12/2012.

[20] Ammunition Program Executive Officer, Picatinny Arsenal, NJ, 07086-5000PEO Ammunition Systems Portfolio Book 2012-2013.

[21] C. Patel et. al., "Qualification of the IM Projectile", IMEMT 2010.

[22] MIL-P-63252A, "Projectile, 155mm, HE, M795 Loading, Assembling and Packing", Images only.

[23] K. D. Laughlin, "Characterization of the Parameters that Affect Projectile Balloting using Finite Element Analysis", Ph.D. Thesis, University of Oklahoma, 2008.

[24] W. Mock et. al., "Dynamic Yield Stress and Elastic Wave Velocity Measurements for HF-1 Steel", Naval Surface Weapons Center report, NSWC TR 3519, September 1976.

[25] W. Mock et. al., "Computational and Experimental Determination of Fragmentation for Naturally Fragmenting Warheads", Naval Surface Weapons Center report, NSWC TR 80-238, May 1981.

[26] W. Mock et. al., "Determination of Dynamic Fracture Parameters for HF-1 Steel", J. Appl. Phys. Vol. 53, No. 8, August 1982, 5660-5668.

[27] W. Mock et. al., "Fragmentation Behavior of Armco Iron and HF-1 Steel Explosive-filled Cylinders", J. Appl. Phys. 54 (5), May 1983, 2344-2351.

[28] W. Mock et. al., "Computation of Fragment Mass Distribution for HF-1 Steel Explosive-filled Cylinders", J. Appl. Phys. 58 (3), August 1985, 1223-1228.

[29] MIL-HDBK-756(AR), Military Handbook, "Manufacture of Projectiles, Projectile Components, and Cartridge Cases for Artillery, Tank Main Armament, and Mortars", Department of Defense, 29 April, 1991.

[30] J. H. Mulherin, "Fracture Mechanics Study on 155 MM M107 Projectile Made from Isothermally Transformed HF-1 Steel", Report Frankford Arsenal, 1976, FA-TR-76015.

[31] D. S. Saunders, "Mechanical Properties and Fracture Toughness Assessment of M795 and M549 155 MM Artillery Projectile Bodies Manufactured from HF-1 Steel", Department of Defense, Materials Research Laboratories, Victoria, Australia, MRL-R-1007, 1986.

[32] J. M. Schreiber, "High-Strain-Rate Property Determination of High-Strength Steel using Finite Element Analysis and Experimental Data", Master Thesis, The Pennsylvania State University, May 2013.

[33] M. Cockcroft et. al, "Ductility and the Workability of Metals" J Inst Metals, 1968. **96**(1): p. 33-39.

[34] NATO, "Procedures for Evaluating the Protection Level of Armoured Vehicles – Volume 3: IED Threat", AEP-55, Edition C Volume 3 (Part I), Version 1, Ratification Draft 1.

[35] M. R. Jensen, "The IMPETUS Afea Solver® - Verification Manual: Defense", CertaSIM report, CS-0021-120114.